Stacking and Solvent Effects on the Electronic and Optical Properties of Gold and Mercury Acetylide Aggregations: A Theoretical Study

Yi Liao[†,‡] and Jing Ma*[,†]

School of Chemistry and Chemical Engineering, Institute of Theoretical and Computational Chemistry, Key Laboratory of Mesoscopic Chemistry of MOE, Nanjing University, Nanjing, 210093, People's Republic of China, and Institute of Functional Material Chemistry, Department of Chemistry, Northeast Normal University, Changchun 130024, People's Republic of China

Received February 22, 2008

The effects of various packing styles, solvents, and substituents on the electronic structures of gold(I) and mercury(II) acetylides are investigated by using the density functional theory (DFT) and the time-dependent density functional theory (TDDFT). In comparison with the second-order Møeller−Plesset (MP2) and coupled-cluster (CCSD(T)) results, most of the hybrid GGA and hybrid meta GGA (among the studied 36 DFT functionals) can give reasonable predictions on binding energies in a dimer. A series of packing aggregates extended along intermolecular Au···Au and $\pi-\pi$ (between aryl ligands) contacting directions are employed to illustrate the stacking dependence of the low-lying vertical excitation energies. The lowest excitation energy undergoes little change from the Au···Au linked dimer to higher oligomers. A polarized continuum model (PCM) study is carried out on a series of substituted gold and mercury acetylide derivatives in several solutions. The lowest vertical excitation energies exhibit a blue shift as the solvent polarity increases. The red shift in the lowest excitation energy is in accordance with the increasing electron-accepting ability of the substituent. The electronic structures of gold acetylides are found to be more sensitive to ligand substitution and solvent polarity than those of the corresponding mercury acetylides.

1. Introduction

Gold(I) and mercury(II) acetylides have attracted growing attention due to their potential applications in the fields of nonlinear optics,[1] liquid crystals,[2] electrical conductors,[3] and luminescent materials.[4] The linearity of the ethyne unit and the preference of a linear dicoordination of the d^{10} metal make alkynyl-gold and -mercury complexes potential precursors for synthesis of organometallic oligomers and polymers.[5] The intermolecular noncovalent interactions, such as π-stacking interactions between aryl ligands of neighboring molecules and weak attractive Au···Au interactions (called aurophilicity), play a crucial role in controlling crystal packing and self-assembly of Au(I) compounds.[6] Although such an aurophilic interaction only has a strength comparable to hydrogen bonding,[7] the cohesive Au···Au interactions in the solid state do exert a marked influence on the overall conformations of gold(I)

* Corresponding author. E-mail: majing@nju.edu.cn.
† Nanjing University.
‡ Northeast Normal University.

(1) (a) Powell, C. E.; Humphrey, M. G. *Coord. Chem. Rev.* **2004**, *248*, 725. (b) Whittall, I. R.; Humphrey, M. G.; Samoc, M.; Lutherdavies, B. *Angew. Chem., Int. Ed. Engl.* **1997**, *36*, 370. (c) Whittall, I. R.; McDonagh, A. M.; Humphrey, M. G.; Samoc, M. *Adv. Organomet. Chem.* **1999**, *43*, 349. (d) Whittall, I. R.; Humphrey, M. G.; Houbrechts, S.; Maes, J.; Persoons, A.; Schmid, S.; Hockless, D. C. R. *J. Organomet. Chem.* **1997**, *544*, 277. (e) Hurst, S. K.; Humphrey, M. G.; Morrall, J. P.; Cifuentes, M. P.; Samoc, M.; Luther-Davies, B.; Heath, G. A.; Willis, A. C. *J. Organomet. Chem.* **2003**, *670*, 56. (f) Humphrey, M. G. *Gold Bull.* **2000**, *33*, 97. (g) Vicente, J.; Singhal, A. R.; Jones, P. G. *Organometallics* **2002**, *21*, 5887. (h) Vicente, J.; Chicote, M. T.; Abrisqueta, M. D.; Ramírez de Arellano, M. C.; Jones, P. G.; Humphrey, M. G.; Cifuentes, M. P.; Samoc, M.; Luther-Davies, B. *Organometallics* **2000**, *19*, 2968.

(2) (a) Alejos, P.; Coco, S.; Espinet, P. *New J. Chem.* **1995**, *19*, 799. (b) Kaharu, T.; Ishii, R.; Adachi, T.; Yoshida, T.; Takahashi, S. *J. Mater.Chem.* **1995**, *5*, 687.

(3) (a) Irwin, M. J.; Gia, G.; Payne, N. C.; Puddephatt, R. J. *Organometallics* **1996**, *15*, 51. (b) Shiotsuka, M.; Yamamoto, Y.; Okuno, S.; Kiton, M.; Nozaki, K.; Onaka, S. *J. Chem. Soc., Chem. Commun.* **2002**, 590.

(4) (a) Long, N. J.; Williams, C. K. *Angew. Chem., Int. Ed.* **2003**, *42*, 2586. (b) Che, C. M.; Yip, H. K.; Lo, W. C.; Peng, S. M. *Polyhedron* **1994**, *13*, 887. (c) Xiao, H.; Cheung, K. K.; Che, C. M. *J. Chem. Soc., Dalton Trans.* **1996**, 3699. (d) Tzeng, B. C.; Lo, W. C.; Che, C. M.; Peng, S. M. *J. Chem. Soc., Chem. Commun.* **1996**, 181. (e) Xiao, H.; Weng, Y. X.; Peng, S. M.; Che, C. M. *J. Chem. Soc., Dalton Trans.* **1996**, 3155. (f) Yam, V. W. W.; Lo, K. K. W.; Wong, K. M. C. *J. Organomet. Chem.* **1999**, *578*, 3. (g) Yip, S. K.; Chan, C. L.; Lam, W. H.; Cheung, K. K.; Yam, V. W. W. *Photochem. Photobiol. Sci.* **2007**, *6*, 365. (h) Yam, V. W. W.; Choi, S. W. K.; Cheung, K. K. *J. Chem. Soc., Dalton Trans.* **1996**, 3411. (i) Yam, V. W. W.; Choi, S. W. K. *J. Chem. Soc., Dalton Trans.* **1996**, 4227. (j) Lu, X. X.; Li, C. K.; Cheng, E. C. C.; Zhu, N. Y.; Yam, V. W. W. *Inorg. Chem.* **2004**, *43*, 2225. (k) Yam, V. W. W.; Yip, S. K.; Yuan, L. H.; Cheung, K. L.; Zhu, N. Y.; Cheung, K. K. *Organometallics* **2003**, *22*, 2630. (l) Hunks, W. J.; MacDonald, M. A.; Jennings, M. C.; Puddephat, R. J. *Organometallics* **2000**, *19*, 5063. (m) Li, P. Y.; Ahrens, B.; Feeder, N.; Raithby, P. R.; Teat, S. J.; Khan, M. S. *J. Chem. Soc., Dalton Trans.* **2005**, 874. (n) Poon, S. Y.; Wong, W. Y.; Cheah, K. W.; Shi, J. X. *Chem. Eur. J.* **2006**, *12*, 2550. (o) Wong, W. Y. *Coord. Chem. Rev.* **2007**, *251*, 2400. (p) Wong, W. Y.; Liu, L.; Shi, J. X. *Angew. Chem., Int. Ed.* **2003**, *42*, 4064. (q) Bolletta, F.; Fabbri, D.; Lombardo, M.; Prodi, L.; Trombini, C.; Zaccheroni, N. *Organometallics* **1996**, *15*, 2415.

(5) (a) Puddephatt, R. J. *Coord. Chem. Rev.* **2001**, *216−217*, 313. (b) Jia, G. C.; Puddephatt, R. J.; Vittal, J. J.; Payne, N. C. *Organometallics* **1993**, *12*, 263. (c) Jia, G. C.; Puddephatt, R. J.; Scott, J. D.; Vittal, J. J. *Organometallics* **1993**, *12*, 3565. (d) Jia, G. C.; Payne, N. C.; Vittal, J. J.; Puddephatt, R. J. *Organometallics* **1993**, *12*, 4771. (e) Lu, W.; Xiang, H. F.; Zhu, N.; Che, C. M. *Organometallics* **2002**, *21*, 2343. (f) Chao, H. Y.; Lu, W.; Li, Y.; Chan, M. C. W.; Che, C. M.; Cheung, K. K.; Zhu, N. *J. Am. Chem. Soc.* **2002**, *124*, 14696. (g) Shieh, S. J.; Hong, X.; Peng, S. M.; Che, C. M. *J. Chem. Soc., Dalton Trans.* **1994**, 3067. (h) Lu, W.; Zhu, N.; Che, C. M. *J. Organomet. Chem.* **2003**, *670*, 11. (i) Liu, L.; Wong, W. Y.; Poon, S. Y.; Shi, J. X.; Cheah, K. W.; Lin, Z. Y. *Chem. Mater.* **2006**, *18*, 1369. (j) Hogarth, G.; Álvarez-Falcón, M. M. *Inorg. Chim. Acta* **2005**, *358*, 1386.

10.1021/om8001697 CCC: $40.75
Publication on Web 08/13/2008

acetylide aggregates, and hence on their optical properties.[8] In contrast, the evidence for Hg···Hg interactions is scarce.[9] A clear picture of the effects of metallophilic interaction, stacking style, and solvation on the electronic structures of gold and mercury acetylides has not yet been established.

With the rapid development of both theoretical methods and computer technology, quantum chemical calculations become useful tools to describe the electronic structures of a hierarchy of oligomers with definite length. There are already some theoretical works on simplified models of monomeric alkynyl gold and mercury complexes, where the PH_3 group is commonly adopted to substitute the PPh_3 ligands for the sake of reducing computational costs.[10a,b] The extended Hückel molecular orbital (EHMO) calculations on PH_3AuCCH[10a] predicted that the lowest excitation was the mixed $\pi\pi^*$ and/or $\sigma\pi^*$ modes. Density functional theory (DFT) calculations with the B3LYP functional were performed on a model system, $H_3PAuC{\equiv}CRC{\equiv}CAuPH_3$,[10b] at the experimental geometry of $Ph_3PAuC{\equiv}CRC{\equiv}CAuPPh_3$. Using the semiemperical EHMO calculations, Che et al.[10d] studied the electronic structure of the $[Au_2(dppm)Ph_2]$ dimer. The conformational and optical properties of mercury diethynylfluorene oligomers were also investigated by using CIS and TD-DFT methods.[10g] However, few theoretical investigations have been performed on higher aggregate oligomers through intermolecular Au···Au or Hg···Hg interactions.

In order to understand the relationship between intermolecular interaction, substitution pattern, solvent media, and the absorption spectra of gold and mercury acetylides, we carried out a systematic study on several models: (1) mononuclear monomers, [(PPh$_3$)Au(C≡C-(C$_4$H$_3$S))] (**Au-M1**) and [(CH$_3$)Hg(C≡C-(C$_4$H$_3$S))] (**Hg-M1**) and the corresponding dimers (**Au-D1**, **Hg-D1**); (2) dinuclear species, monomers [RM (C≡C-(C$_4$H$_2$S)-C≡C) MR] (**Au-M2**−**Au-M5**, M = Au, R = PPh_3, PMe_3, PH_3, and PF_3; **Hg-M2**−**Hg-M5**, M = Hg, R = Ph, Me, H, and F) and dimers [RM (C≡C-(C$_4$H$_2$S)-C≡C) MR]$_2$ (**Au-D2**, M = Au, R = PPh_3; **Hg-D2**, M = Hg, R = Me); (3) the stacking oligomers along Au···Au contacts (**A$_n$**) and $\pi-\pi$ interactions between triphenylphosphine rings (**B$_n$**), and the mixed (**AB**) directions in the crystal structure, respectively; and (4) solvent models for monomers and dimers in various solvents, as shown in Figure 1. On the basis of these models, we apply various theoretical methods to investigate the binding energy, the intra- and intermolecular interactions, stacking, substituent, and solvent effects on the low-lying vertical excitation energies. The results may provide new insight into the nature of the intermolecular interactions of gold(I) and mercury(II) acetylide complexes in crystal and solutions.

2. Computational Details and Models

DFT Functionals. All calculations were performed with Gaussian 03 program.[11] The performances of 36 fucntionals, belonging to four categories of DFT functionals, were tested in calculations of intermolecular binding energy of a simplified model of mononuclear gold acetylide (**Au-D1**), with three phenyl groups substituted by hydrogen atoms, respectively. The tested functionals include (1) generalized gradient approximation (GGA), BLYP, BP86, BPBE, BPW91, HCTH, G96LYP, MPWLYP, MPWPBE, MPWPW91, OLYP, and PBE; (2) hybrid GGA methods, B3LYP, B3P86, B3PW91, B97-1, B97-2, B98, BHandHLYP, MPW1LYP, MPW3LYP, O3LYP, PBE1PBE, and X3LYP; (3) meta GGA, BB95, MPWB95, MPWKCIS, PBEKCIS, and VSXC; and (4) hybrid meta GGA, B1B95, BB1K, MPW1B95, MPW1KCIS, MPWB1K, MPWKCIS1K, and PBE1KCIS. The details of these selected DFT functionals are summarized in Table S1 of the Supporting Information. Since experimental binding energy of alkynyl gold is not available, we also used the second-order Møeller−Plesset method (MP2)[12] and coupled-cluster (CCSD(T))[13] calculations for comparison. As shown in Figure 2, the binding energies, with the basis set superposition error (BSSE) corrections, obtained by most of the hybrid GGA and hybrid meta GGA (where "meta" means the functional depends on the Kohn−Sham orbitals in the form of a kinetic energy density) are comparable to MP2 and CCSD(T) values. Furthermore, one of the hybrid GGA

(6) (a) Che, C. M.; Chao, H. Y.; Miskowski, V. M.; Li, Y. Q.; Cheung, K. K. *J. Am. Chem. Soc.* **2001**, *123*, 4985. (b) Lu, W.; Zhu, N. Y.; Che, C. M. *J. Am. Chem. Soc.* **2003**, *125*, 16081. (c) Fu, W. F.; Chan, K. C.; Miskowski, V. M.; Che, C. M. *Angew. Chem., Int. Ed.* **1999**, *38*, 2783. (d) Yam, V. W. W.; Li, C. K.; Chan, C. L. *Angew. Chem., Int. Ed.* **1998**, *37*, 2857. (e) Tang, H. S.; Zhu, N. Y.; Yam, V. W. W. *Organometallics* **2007**, *26*, 22. (f) Vicente, J.; Chicote, M. T.; Alvarez-Falcón, M. M.; Jones, P. G. *Organometallics* **2005**, *24*, 2764. (g) Vicente, J.; Chicote, M. T.; Alvarez-Falcón, M. M.; Fox, M. A.; Bautista, D. *Organometallics* **2003**, *22*, 4792. (h) Vicente, J.; Chicote, M. T.; Alvarez-Falcón, M. M.; Jones, P. G. *Organometallics* **2005**, *24*, 5956. (i) Vicente, J.; Chicote, M. T.; Alvarez-Falcón, M. M. *Organometallics* **2004**, *23*, 5707. (j) White-Morris, R. L.; Olmstead, M. M.; Balch, A. L. *J. Am. Chem. Soc.* **2003**, *125*, 1033. (k) Stork, J. R.; Rios, D.; Pham, D.; Bicocca, V.; Olmstead, M. M.; Balch, A. L. *Inorg. Chem.* **2005**, *44*, 3466. (l) Schneider, W.; Bauer, A.; Schmidbaur, H. *Organometallics* **1996**, *15*, 5445.

(7) (a) Schmidbaur, H. *Chem. Soc. Rev.* **1995**, *24*, 391. (b) Schmidbaur, H. *Gold Bull.* **1990**, *23*, 11. (c) Schmidbaur, H.; Graf, W.; Müller, G. *Angew. Chem., Int. Ed. Engl.* **1988**, *27*, 417. (d) Harwell, D. E.; Mortimer, M. D.; Knobler, C. B.; Anet, F. A. L.; Hawthorne, M. F. *J. Am. Chem. Soc.* **1996**, *118*, 2679. (e) Tang, S. S.; Chang, C. P.; Lin, I. J. B.; Liou, L. S.; Wang, J. C. *Inorg. Chem.* **1997**, *36*, 2294. (f) Pyykkö, P.; Mendizabal, F. *Inorg. Chem.* **1998**, *37*, 3018.

(8) (a) Li, P.; Ahrens, B.; Choi, K. H.; Khan, M. S.; Raithby, P. R.; Wilson, P. J.; Wong, W. Y. *CrystEngComm* **2002**, *4*, 405. (b) McArdle, C. P.; Irwin, M. J.; Jennings, M. C.; Puddephatt, R. J. *Angew. Chem., Int. Ed.* **1999**, *38*, 3376. (c) MacDonald, M. A.; Puddephatt, R. J.; Yap, G. P. A. *Organometallics* **2000**, *19*, 2194. (d) Puddephatt, R. J. *Chem. Commun.* **1998**, 1055. (e) Li, D.; Hong, X; Che, C. M.; Lo, W. C.; Peng, S. M. *J. Chem. Soc., Dalton Trans.* **1993**, 2929. (f) Fu, W. F.; Chan, K. C.; Cheung, K. K.; Che, C. M. *Chem.−Eur. J.* **2001**, *7*, 4656. (g) Yam, V. W. W.; Choi, S. W. K.; Cheung, K. K. *Organometallics* **1996**, *15*, 1734. (h) Liau, R. Y.; Schier, A.; Schmidbaur, H. *Organometallics* **2003**, *22*, 3199. (i) Vicente, J.; Chicote, M. T.; Alvarez-Falcón, M. M.; Jones, P. G. *Organometallics* **2005**, *24*, 4666.

(9) (a) Pyykkö, P. *Chem. Rev.* **1997**, *97*, 597. (b) Mingos, D. M. P.; Vilar, R.; Rais, D. *J. Organomet. Chem.* **2002**, *641*, 126.

(10) (a) Irwin, M. J.; Vittal, J. J.; Puddephatt, R. J. *Organometallics* **1997**, *16*, 3541. (b) Wong, W. Y.; Choi, K. H.; Lu, G. L.; Shi, J. X.; Lai, P. Y.; Chan, S. M.; Lin, Z. *Organometallics* **2001**, *20*, 5446. (c) Brandys, M. C.; Jennings, M. C.; Puddephatt, R. J. *J. Chem. Soc., Dalton Trans.* **2000**, 4601. (d) Hong, X.; Cheung, K. K.; Che, C. M. *J. Chem. Soc., Dalton Trans.* **1994**, 1867. (e) Yip, S. K.; Lan, W. H.; Zhu, N. Y.; Yam, V. W. W. *Inorg. Chim. Acta* **2006**, *359*, 3639. (f) King, C.; Wang, J. C.; Khan, M. N. I.; Fackler, J. P., Jr. *Inorg. Chem.* **1989**, *28*, 2145. (g) Liao, Y.; Feng, J. K.; Yang, L.; Ren, A. M.; Zhang, H. X. *Organometallics* **2005**, *24*, 385.

(11) Frisch, M. J.; Trucks, G. W.; Schlegel, H. B.; Scuseria, G. E.; Robb, M. A.; Cheeseman, J. R.; Montgomery, J. A., Jr.; Vreven, T.; Kudin, K. N.; Burant, J. C.; Millam, J. M.; Iyengar, S. S.; Tomasi, J.; Barone, V.; Mennucci, B.; Cossi, M.; Scalmani, G.; Rega, N.; Petersson, G. A.; Nakatsuji, H.; Hada, M.; Ehara, M.; Toyota, K.; Fukuda, R.; Hasegawa, J.; Ishida, M.; Nakajima, T.; Honda, Y.; Kitao, O.; Nakai, H.; Klene, M.; Li, X.; Knox, J. E.; Hratchian, H. P.; Cross, J. B.; Adamo, C.; Jaramillo, J.; Gomperts, R.; Stratmann, R. E.; Yazyev, O.; Austin, A. J.; Cammi, R.; Pomelli, C.; Ochterski, J. W.; Ayala, P. Y.; Morokuma, K.; Voth, G. A.; Salvador, P.; Dannenberg, J. J.; Zakrzewski, V. G.; Dapprich, S.; Daniels, A. D.; Strain, M. C.; Farkas, O.; Malick, D. K.; Rabuck, A. D.; Raghavachari, K.; Foresman, J. B.; Ortiz, J. V.; Cui, Q.; Baboul, A. G.; Clifford, S.; Cioslowski, J.; Stefanov, B. B.; Liu, G.; Liashenko, A.; Piskorz, P.; Komaromi, I.; Martin, R. L.; Fox, D. J.; Keith, T.; Al-Laham, M. A.; Peng, C. Y.; Nanayakkara, A.; Challacombe, M.; Gill, P. M. W.; Johnson, B.; Chen, W.; Wong, M. W.; Gonzalez, C.; Pople, J. A. *Gaussian 03*, revision B.04; Gaussian, Inc.: Wallingford, CT, 2004.

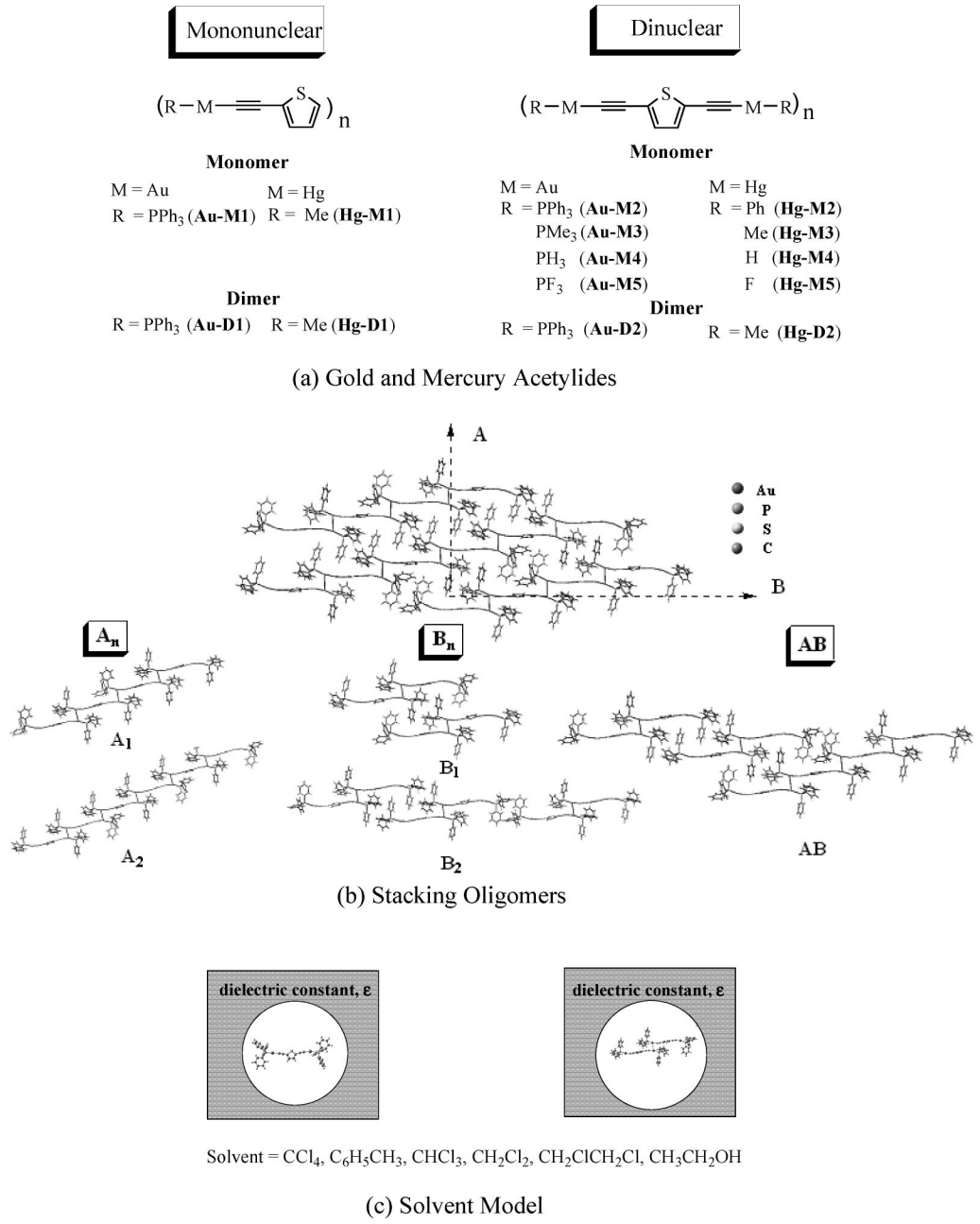

Figure 1. The studied models of (a) the mononuclear (monomer, **Au-M1** and **Hg-M1**; dimer, **Au-D1** and **Hg-D1**) and diunclear gold(I) and mercury(II) acetylides (monomers, **Au-M2**−**Au-M5** and **Hg-M2**−**Hg-M5**; dimer, **Au-D2** and **Hg-D2**), and (b) two-dimensional crystal stacking of triphenylphosphine gold acetylide with the X-ray structure taken from ref 8a. Each molecule is surrounded by its neighbors with the contact of Au···Au (**An**), $\pi-\pi$ (**Bn**), and their mixture (**AB**) of directions, respectively. (c) Solvent models of monomers and dimers in various solvents.

functionals, Becke's three-parameter hybrid method[14] using the Perdew and Wang correlation functional (B3PW91),[15] was employed in our calculations of electronic structures of monomers and dimers under vacuum, X-ray structures, and various solvents. The PW91 functional was also found to perform reasonably for gold clusters in other works.[16]

Basis Sets. Two sets of effective core potentials (ECP) were employed for Au (or Hg) atoms. The first one was Los Alamos ECP, Lanl2dz, from Hay and Wadt.[17] The second one employed the ECP60MWB pseudopotential of the Stuttgart/Bonn group.[18] For all other nonmetallic elements, standard Gaussian basis sets 3-21G*, 6-31G*, and 6-31+G* were adopted, respectively. Therefore, in total four suites of basis sets were used in the present calculations, denoted as BAS1 (LanL2DZ (8s6p3d)/[3s3p2d] for Au and (3s3p3d)/[2s2p2d] for Hg; 3-21G* for nonmetal atoms),

(12) Head-Gordon, M.; Pople, J. A.; Frisch, M. J. *Chem. Phys. Lett.* **1988**, *153*, 503.
(13) Pople, J. A.; Head-Gordon, M.; Raghavachari, K. *J. Chem. Phys.* **1987**, *87*, 5968.
(14) (a) Becke, A. D. *J. Chem. Phys.* **1993**, *98*, 5648. (b) Becke, A. D. *Phys. Rev. A* **1988**, *38*, 3089. (c) Becke, A. D. *J. Chem. Phys.* **1993**, *98*, 1372.
(15) (a) Perdew, J. P.; Chevary, J. A.; Vosko, S. H.; Jackson, K. A.; Pederson, M. R.; Singh, D. J.; Fiolhais, C. *Phys. Rev. B* **1992**, *46*, 6671. (b) Perdew, J. P.; Chevary, J. A.; Vosko, S. H.; Jackson, K. A.; Pederson, M. R.; Singh, D. J.; Fiolhais, C. *Phys. Rev. B* **1993**, *48*, 4978. (c) Perdew, J. P.; Burke, K.; Wang, Y. *Phys. Rev. B* **1996**, *54*, 16533.
(16) (a) Wu, X.; Senapati, L.; Nayak, S. K.; Selloni, A.; Hajaligol, M. *J. Chem. Phys.* **2002**, *117*, 4010. (b) Li, G. P.; Hamilton, I. P. *Chem. Phys. Lett.* **2006**, *420*, 474.

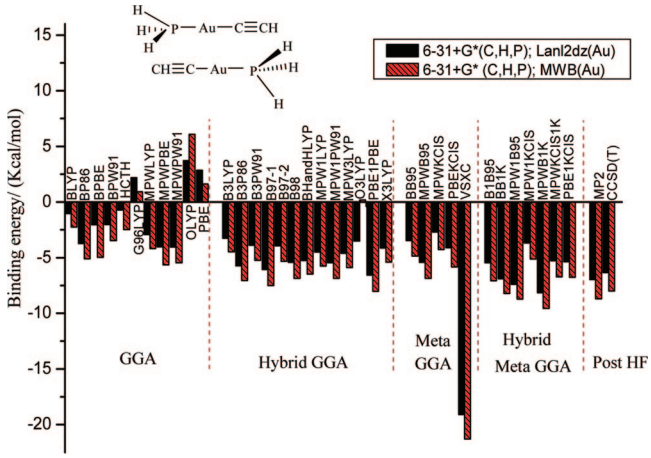

Figure 2. Binding energies (kcal/mol) with BSSE corrections of $(PH_3AuC{\equiv}CH)_2$, obtained by using various theoretical methods, with the geometry taken form the X-ray structure of **Au-D1**.

BAS2 (LanL2DZ for Au and Hg; 6-31G* for others), BAS3 (LanL2DZ for Au; 6-31+G* for others), and BAS4 (ECP60MWB (8s7p6d)/[6s5p3d] basis sets for Au; 6-31+G* for others), respectively. The geometry optimizations of monomers were performed with the medium level of basis set, BAS2. The larger basis sets, BAS3 and BAS4, were applied to calculations of binding energy in a dimer, respectively (Figure 2). Limited by the computational cost, the relatively lower basis set, BAS1, was applied to calculate the absorption spectra of the studied oligomers.

Intermolecular Interactions. Natural bond orbital analysis (NBO)[19] was performed to provide a qualitative description of intra- and intermolecular interactions, such as ligand-to-metal and metal−metal interactions. Interaction energies between fragments can be computed by using the NBO Fock matrix deletion procedure.[20]Three kinds of density functionals, hybrid GGA (B97-1), meta GGA (MPWB95), and hybrid meta GGA (BB1K), were adopted in the NBO deletion procedure, respectively. Similar results of intra- and intermolecular interactions are obtained by using these different sets of DFT functionals (Figure 3).

Absorption Spectra. The vertical excitation energies were calculated within the framework of time-dependent density functional theory (TD-DFT),[21] an effective way to calculate the low-lying excitation energies of some organometallic complexes.[22] The basis set selected was LanL2DZ for Au (or Hg) and 3-21G* for others. The spin−orbit interactions are not included in the present work, as done in a previous study on diethynylfluorenyl gold complexes.[23] It was shown that the spin−orbit effects were insignificant in some other Au(I) systems.[24]

Solvent Model. Solvent effects on TDDFT excitation energies were also considered in the framework of the self-consistent reaction field polarizable continuum model (SCRF-PCM)[25] by using the united atom topological model (UAHF) set of solvation radii to build the cavity for the solute. The TDDFT/PCM was widely applied to calculate the low-lying vertical excitation energies of some organic and organometallic systems in nonpolar and weakly polar solvents.[26]

3. Results and Discussion

3.1. Intermolecular vs Intramolecular Interactions. Intramolecular Interaction. In order to understand the intramolecular interactions in gold(I) and mercury(II) acetylides, we have performed the NBO analysis of model systems **Au-M1** and **Hg-M1**, respectively. The relative magnitudes of intramolecular interactions, obtained by using B97-1, BB1K, and MPWB95 functionals, respectively, are depicted in Figure 3. These three kinds of DFT functionals give similar results. The intramolecular interactions between the PPh_3 fragment and gold acetylene within **Au-M1** (with the total interaction energy of −267 kcal/mol at the level of BB1K/LanL2DZ for Au and 6-31G* for others) mainly have the characteristic of σ donation, $n_P \rightarrow \sigma^*_{Au\text{-}c}$, from the lone pair orbital of the P atom, n_P, to the antibonding orbital of Au−C, $\sigma^*_{Au\text{-}c}$. The relatively weaker back-donation from the d orbitals of the Au atom to vacant p orbitals of the P atom and the antibonding σ orbital of P−C, σ^*_{P-C}, respectively, also contributes to the intramolecular interactions in **Au-M1**. In comparison with **Au-M1**, it is apparent that **Hg-M1** has stronger intramolecular σ donation from the ligand fragment to the metal with a total interaction energy of −374 kcal/mol at the BB1K level.

Intermolecular Interaction. The NBO results of intermolecular interactions in the dimers **Au-D1** and **Hg-D1** are listed in Table 1. The total intermolecular interaction in **Au-D1** is −33 kcal/mol, about one-tenth of that of intramolecular interac-

(17) (a) Hay, P. J.; Wadt, W. R. *J. Chem. Phys.* **1985**, *82*, 270. (b) Wadt, W. R.; Hay, P. J. *J. Chem. Phys.* **1985**, *82*, 284. (c) Hay, P. J.; Wadt, W. R. *J. Chem. Phys.* **1985**, *82*, 299.

(18) Andrae, D.; Haeussermann, U.; Dolg, M.; Stoll, H.; Preuss, H. *Theor. Chim. Acta* **1990**, *77*, 123.

(19) Glendening, E. D.; Reed, A. E.; Carpenter, J. E.; Weinhold, F. *NBO*, Version 3.1; Gaussian, Inc.: Pittsburgh, PA, 2003.

(20) (a) Reed, A. E.; Curtiss, L. A.; Weinhold, F. *Chem. Rev.* **1988**, *88*, 899. (b) Montejo, M.; Navarro, A.; Kearley, G. J.; Vázquez, J.; López-González, J. J. *J. Am. Chem. Soc.* **2004**, *126*, 15087.

(21) (a) Casida, M. K.; Jamorski, C.; Casida, K. C.; Salahub, D. R. *J. Chem. Phys.* **1998**, *108*, 4439. (b) Stratmann, R. E.; Scuseria, G. E. *J. Chem. Phys.* **1998**, *109*, 8218.

(22) See, for example:(a) Pan, Q. J.; Zhang, H. X.; Fu, H. G.; Yu, H. T. *Eur. J. Inorg. Chem.* **2006**, 1050. (b) Zhou, X.; Pan, Q. J.; Xia, B. H.; Li, M. X.; Zhang, H. X.; Tung, A. C. *J. Phys. Chem. A* **2007**, *111*, 5465. (c) Li, M. X.; Zhang, H. X.; Zhou, X.; Pan, Q. J.; Fu, H. G.; Sun, C. C. *Eur. J. Inorg. Chem.* **2007**, 2171. (d) Pan, Q. J.; Zhou, X.; Zhang, H. X.; Fu, H. G. *J. Photochem. Photobiol. A* **2007**, *188*, 287. (e) Pan, Q. J.; Zhou, X.; Yu, H. T.; Zhang, H. X.; Fu, H. G. *Inorg. Chem. Commun.* **2007**, *10*, 183. (f) Liu, T.; Gao, J. S.; Xia, B. H.; Zhou, X.; Zhang, H. X. *Polymer* **2007**, *48*, 502. (g) Pan, Q. J.; Zhang, H. X.; Fu, H. G.; Yu, H. T. *Eur. J. Inorg. Chem.* **2006**, 1050. (h) Charmant, J. P. H.; Forniés, J.; Gómez, J.; Lalinde, E.; Merino, R. I.; Moreno, M. T.; Orpen, A. G. *Organometallics* **2003**, *22*, 652. (i) Rosa, A.; Baerends, E. J.; van Gisbergen, S. J. A.; van Lenthe, E.; Gooeneveld, J. A.; Snihders, J. G. *J. Am. Chem. Soc.* **1999**, *121*, 10356. (j) Adamo, C.; Barone, V. *Theo. Chem. Acc.* **2000**, *105*, 169. (k) Boulet, P.; Chermett, H.; Daul, C.; Gilardoni, F.; Rogemond, F.; Weber, J.; Zuber, G. *J. Phys. Chem. A* **2001**, *105*, 885. (l) Farrell, I. R.; van Slageren, J.; Zalis, S.; Vlcek, A. *Inorg. Chim. Acta* **2001**, *315*, 44. (m) Stoyanov, S. R.; Villegas, J. M.; Rillema, D. P. *Inorg. Chem.* **2003**, *42*, 7852. (n) Halls, M. D.; Schlegel, H. B. *Chem. Mater.* **2001**, *13*, 2632. (o) Martin, R. L.; Kress, J. D.; Campbell, I. H. *Phys. Rev. B* **2000**, *61*, 15804. (p) Han, Y. K.; Lee, S. U. *Chem. Phys. Lett.* **2002**, *366*, 9.

(23) Liao, Y.; Yang, G. C.; Feng, J. K.; Shi, L. L.; Yang, S. Y.; Yang, L.; Ren, A. M. *J. Phys. Chem. A* **2006**, *110*, 13036.

(24) (a) Fang, H.; Wang, S. G. *J. Mol. Model.* **2007**, *13*, 255. (b) Van Lenthe, E.; Snijders, J. G.; Baerends, E. J. *J. Chem. Phys.* **1996**, *105*, 6505. (c) Wang, S. G.; Schwarz, W. H. E. *J. Am. Chem. Soc.* **2004**, *126*, 1266.

(25) (a) Miertus, S.; Scrocco, E.; Tomasi, J. *Chem. Phys.* **1981**, *55*, 117. (b) Miertus, S.; Tomasi, J. *Chem. Phys.* **1982**, *65*, 239. (c) Cossi, M.; Barone, V.; Cammi, R.; Tomasi, J. *Chem. Phys. Lett.* **1996**, *255*, 327. (d) Cancès, M. T.; Mennucci, B.; Tomasi, J. *J. Chem. Phys.* **1997**, *107*, 3032.

(26) See, for example:(a) Tomasi, J.; Mennucci, B.; Cammi, R. *Chem. Rev.* **2005**, *105*, 2999. (b) Tomasi, J.; Persico, M. *Chem. Rev.* **1994**, *94*, 2027. (c) Barone, V; Cossi, M.; Tomasi, J. *J. Chem. Phys.* **1997**, *107*, 3210. (d) Meng, S. C.; Ma, J.; Jiang, Y. S. *J. Phys. Chem. B* **2007**, *111*, 4128. (e) Freccero, M.; Fasani, E.; Mella, M.; Manet, I.; Monti, S.; Albini, A. *Chem.−Eur. J.* **2008**, *14*, 653. (f) Cossi, M.; Barone, V. *J. Chem. Phys.* **2001**, *115*, 4708. (g) Pan, Q. J.; Zhang, H. X.; Zhou, X.; Fu, H. G.; Yu, H. T. *J. Phys. Chem. A* **2007**, *111*, 287. (h) Liu, T.; Xia, B. H.; Zhou, X.; Zhang, H. X.; Pan, Q. J.; Gao, J. S. *Organometallics* **2007**, *26*, 143. (i) Pan, Q. J.; Fu, H. G.; Yu, H. T.; Zhang, H. X. *Inorg. Chem.* **2006**, *45*, 8729.

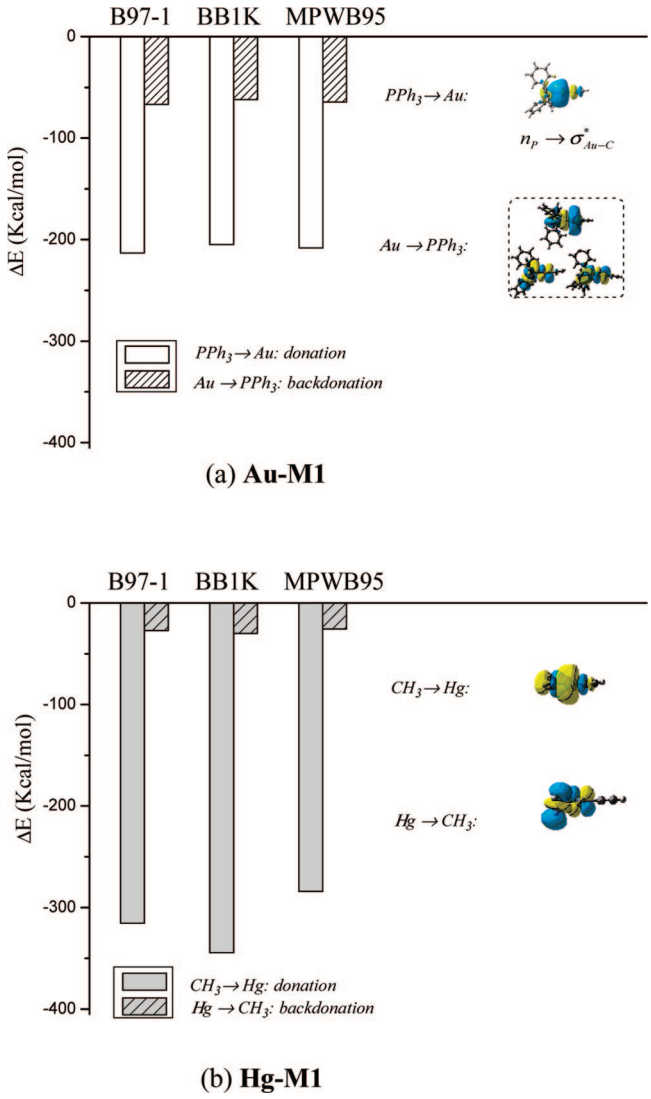

Figure 3. Natural bond orbital (NBO) analysis of intramolecular interactions in [(PPh$_3$)Au(C≡C-(C$_4$H$_3$S))], **Au-M1**, and [(CH$_3$)Hg(C≡C-(C$_4$H$_3$S))], **Hg-M1**, obtained by using B97-1, BB1K, and MPWB95 functionals, respectively, with LanL2DZ for Au or Hg and 6-31G* for others. The isodensity value is 0.02 e·bohr^{-3} for the plotted orbitals.

tion in the constituent monomer (**Au-M1**). As depicted in Table 1, the major intermolecular interactions in **Au-D1** consist of metal−metal and metal−ligand interactions between neighboring molecules. The aurophilic Au···Au interaction (−23 kcal/mol) is slightly larger than the electron delocalization from the ligand to the metal (−9.9 kcal/mol) in another chain. Early studies based on EHMO[10d] and SCF-Xα-SW calculations[10f] ascribed such attractive interactions between two d^{10} closed-shell configurations of Au(I) centers to the mixing of empty metal s and p orbitals into the d shell. In our calculations, significant intermolecular interactions between the σ_{Au-C} bonding orbital (or 5d orbitals) of the Au atom and the antibonding σ^*_{Au-C} orbital of an adjacent molecule are found in the stacking dimer. Although similar intermolecular metallophilic interactions (σ_{Hg-C} or $d_{Hg}\rightarrow\sigma^*_{Hg-C}$) are also observed in **Hg-D1**, the magnitude of mercurophilic interactions (−0.26 kcal/mol) is only about 1% of the aurophilic interactions (−23 kcal/mol) in **Au-D1**. This may be partially rationalized by the much larger energy gap (0.70 or 0.53 eV) between the electron-donating (d_{Hg} or σ_{Hg-C}) and accepting (σ^*_{Hg-C}) orbitals in mercury acetylides than those (0.44, 0.30 eV) in corresponding gold acetylides. It is also interesting to note that in **Hg-D1** the magnitude of intermolecular Hg···Hg interactions (−0.26 kcal/mol) is much lower than that of the intermolecular Hg···ligand interactions (−10.3 kcal/mol). Therefore, the assignment of such a close Hg···Hg separation (about 3.93 Å) to mercurophilicity is still open to debate; the distinct intermolecular interactions between ligand−ligand moieties or Hg−ligand might be responsible for the close contact of the metal centers, as addressed before.[27]

Table 1. Natural Bond Orbital (NBO) Analysis of Intermolecular Metal−Metal (M↔M′) and Metal−Ligand (M↔L) Interactions in [(PPh$_3$)Au(C≡C-(C$_4$H$_3$S))]$_2$ (Au-D1) and [(CH$_3$)Hg(C≡C-(C$_4$H$_3$S))]$_2$ (Hg-D1)[a]

	Metal-Metal interaction (M↔M')		Metal-Ligand interaction (M↔L)	
	M = Au, Ligand = PPh$_3$ (**Au-D1**)			
Orbital interaction				
	$\sigma_{Au-C}\rightarrow\sigma^*_{Au-C}$	$d_{Au}\rightarrow\sigma^*_{Au-C}$	$\pi_{CC}\rightarrow\sigma^*_{C-H}$	$n_P\rightarrow 6p_{Au}$
Interaction energy (Kcal/mol)	-2.82	-1.01	-0.62	-1.58
	M = Hg, Ligand = Me (**Hg-D1**)			
Orbital interaction		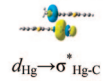		
	$\sigma_{Hg-C}\rightarrow\sigma^*_{Hg-C}$	$d_{Hg}\rightarrow\sigma^*_{Hg-C}$	$\sigma_{Hg-C}\rightarrow 6p_{Hg}$	$n_S\rightarrow\sigma^*_{CH}$
Interaction energy (Kcal/mol)	-0.06	-0.07	-2.29	-1.07

[a] The results are obtained by using the BB1K functional with LanL2DZ for Au and Hg and 6-31G* for others. The isodensity value is 0.02 e·bohr^{-3} for the plotted orbitals.

3.2. Excitation Energies. 3.2.1. Monomers in Gas-Phase and Crystal Structures. In order to assess the extent to which the optical properties are affected by intermolecular interactions in the solid state, TDDFT calculations of gold(I) and mercury(II) acetylides are performed at the level of B3PW91/BAS1 (LanL2DZ for Au and Hg; 3-21G* for others) on the basis of gas-phase and crystal structures, respectively. The effects of ligand modification and metal substitution are also considered in this subsection.

Geometry. The gas-phase geometries of the studied gold(I) acetylide (**Au-M2**−**Au-M5**) and mercury(II) acetylide derivatives (**Hg-M2**−**Hg-M5**) are shown in Table S2. All these molecules exhibit a rod-like geometry with the two-coordinated Au(I) or Hg(II) center adopting a near-linear geometry. The optimized geometries of all these systems vary slightly upon modification of the ligand and metal center. The changes in bond lengths from **Au-M2** (**Hg-M2**) to **Au-M5** (**Hg-M5**) are no more than 0.04 Å, and the variations in angles are within 3°.

Comparing with available experimental data, the geometries of **Hg-M3** optimized by B3PW91 are close to those from electron diffraction experiments,[28] while the optimized geometries of **Au-M2** differ from the experimental data in P−C bond lengths of PPh$_3$ segments and angles of the metal-ethynyl part.[8a] In the gas phase, the phosphine centers predicted by B3PW91 have an approximate C_3 symmetry with three nearly identical P−C(phenyl) bond lengths of 1.8 Å. But in the case of crystal

(27) Schmidbaur, H.; Öller, H. J.; Wilkinson, D. L.; Huber, B.; Müller, G. *Chem. Ber.* **1989**, *122*, 31.
(28) Wong, W. Y.; Choi, K. H.; Lu, G. L.; Lin, Z. Y. *Organometallics* **2002**, *21*, 4475.

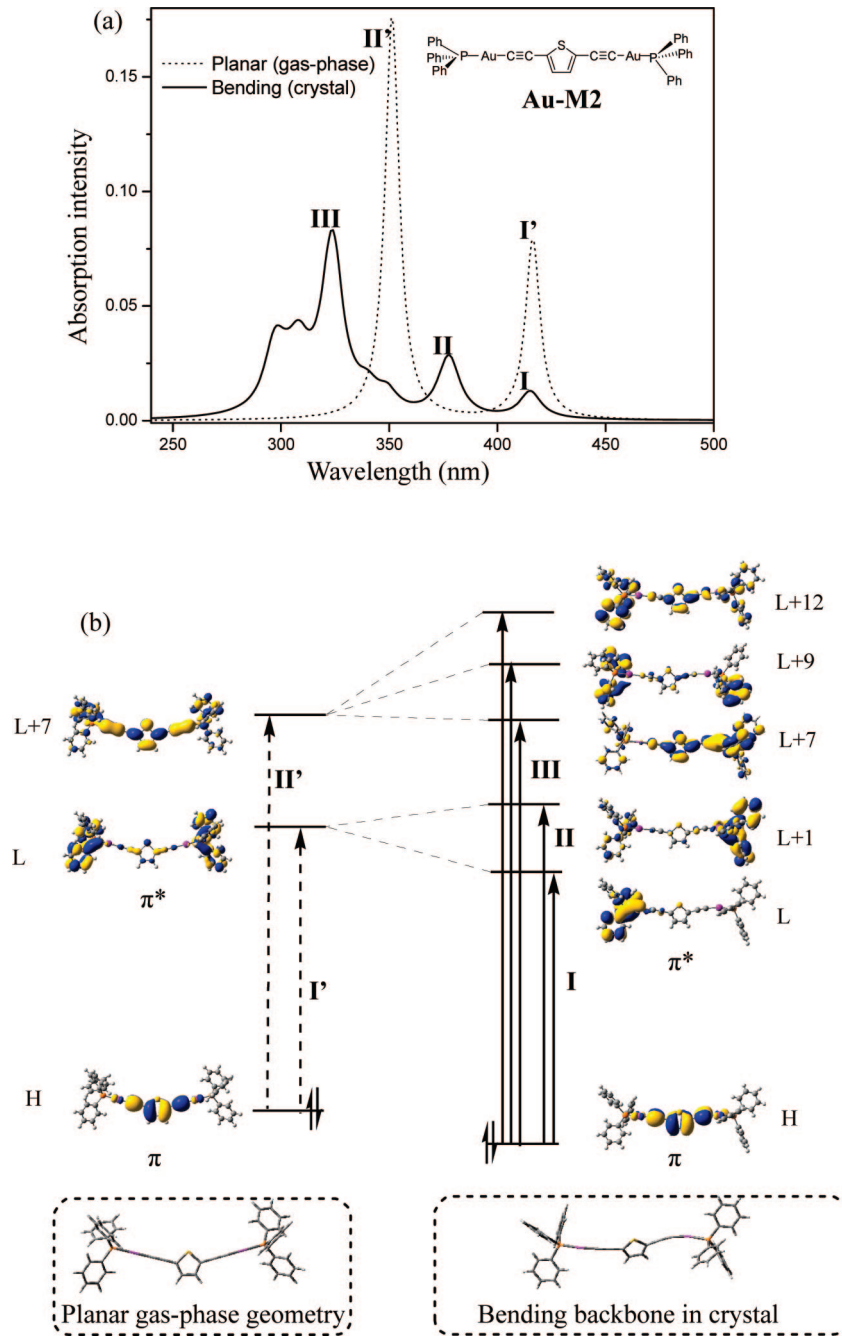

Figure 4. (a) UV−vis absorption spectra of dinuclear gold phosphine acetylide monomer (**Au-M2**) in the optimized gas-phase structure (dotted line) and X-ray crystal structure (solid line). The absorption spectra were simulated by using a Lorentzian convolution with 20 nm half-widths. (b) Frontier molecular orbitals and electronic transition of **Au-M2** at the optimized gas-phase structure (left) and crystal structure (right), respectively. H and L denote the highest occupied and lowest unoccupied molecular orbitals, respectively.

packing, the corresponding PPh_3 fragments possess C_1 symmetry with different P−C(phenyl) crystal bond lengths of 1.7, 1.8, and 1.9 Å, respectively. Accordingly, the bond angles in the metal-ethynyl part of the crystal structure prefer a deviation from linearity of about 15° instead of the ideal planar structure in the gas phase. In other words, the molecular backbone of alkynyl gold phosphine is slightly distorted into an asymmetric form in the solid state, resulting in shifts of the absorption spectra from the gas-phase isolated monomer to the packing systems (as demonstrated below).

Absorption Spectra. The TDDFT vertical excitation energies of monomers, **Au-M2** and **Hg-M3**, in both the gas-phase and crystal structures are obtained at the B3PW91 level with the LanL2DZ basis set for Au (or Hg) and 3-21G* for others. The detailed results of the low-lying excitation energies (E_{ex}) and oscillator strengths (f) are given in Table S3 and Figure S1a of the Supporting Information. Similar absorption spectra are observed for **Hg-M3** in the gas phase and crystal owning to their nearly identical geometry (Figure S1). As expected, the difference in the ground-state geometry of **Au-M2** in the gas phase and crystal brings about evident differences in the band shape, peak positions, and relative intensity of absorption spectra, as plotted in Figure 4. For **Au-M2** in the optimized gas-phase structure, two main absorption bands at 416 nm (I′) and 351 nm (II′) are predicted (dotted line). But three relatively weaker bands at 415 nm (I), 377 nm (II), and 323 nm (III) are observed for **Au-M2** in the crystal structure (solid line). The lowest energy absorption band (I′)

Table 2. Lowest Singlet Excitation Energies (nm) for Gold and Mercury Acetylide Monomers in the Gas Phase and Several Solvents with B3PW91/BAS1-Optimized Structures

	Excitation energy (nm)					
media	TD-DFT/PCM	expt.	band[a]	media	TD-DFT/PCM	expt.	band[a]
	Au-M2 (R=PPh_3)				**Hg-M2** (R=Ph)		
Gas	416.4		I′	Gas	328.1		II′
	351.0		II′				
CCl_4	374.1		II′	CCl_4	327.6		II′
$CHCl_3$	360.7		II′	$CHCl_3$	323.4		II′
CH_2Cl_2	355.0	354[b]	II′	CH_2Cl_2	321.9	341[c]	II′
	Au-M3 (R=PMe_3)				**Hg-M3** (R=Me)		
Gas	365.5		II′	Gas	326.2		II′
CCl_4	359.6		II′	CCl_4	326.6		II′
$CHCl_3$	353.4		II′	$CHCl_3$	322.8		II′
CH_2Cl_2	350.2		II′	CH_2Cl_2	321.3	337[c]	II′
	Au-M4 (R=PH_3)				**Hg-M4** (R=H)		
Gas	377.0		II′	Gas	330.0		II′
CCl_4	366.2		II′	CCl_4	328.5		II′
$CHCl_3$	357.6		II′	$CHCl_3$	323.6		II′
CH_2Cl_2	352.3		II′	CH_2Cl_2	321.9		II′
	Au-M5 (R=PF_3)				**Hg-M5** (R=F)		
Gas	403.6		II′	Gas	314.7		II′
CCl_4	389.9		II′	CCl_4	318.4		II′
$CHCl_3$	377.2		II′	$CHCl_3$	316.1		II′
CH_2Cl_2	362.3		II′	CH_2Cl_2	315.2		II′

[a] The classification of adsorption bands is given in Figure4. [b] Absorption maximum measured in CH_2Cl_2 for mononuclear gold acetylide [$(PPh_3)Au(C{\equiv}C(C_4H_2S)(C_4H_3S))$], obtained from ref 8a. [c] Taken from ref 28.

of **Au-M2** in the gas-phase structure is mainly ascribed to the transition from the HOMO to LUMO. As shown in Figure 4b, the HOMO consists of a π-bonding orbital of the ligand, mixing with 5d orbitals of the Au atom. The LUMO belongs to a π^*-antibonding orbital, which is delocalized over the whole molecule. Thus, the band I′ can be assigned as the ligand-to-ligand charge transfer (LLCT), $\pi\rightarrow\pi^*$, mixing with d(Au)$\rightarrow\pi^*$ metal-to-ligand charge transfer (MLCT). Changing from the gas-phase to solid-state structures, the lowest energy $\pi\rightarrow\pi^*$ transition (I′) is split into two $\pi\rightarrow\pi^*$ transitions, corresponding to bands I and II, respectively (Figure 4a). It can be also found that on going from the linear gas-

Scheme 1

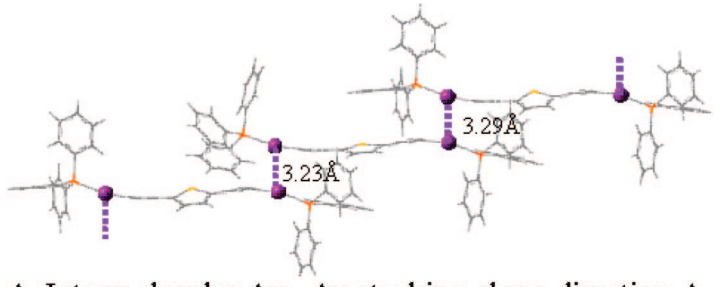

A. Intermolecular Au···Au stacking along direction A

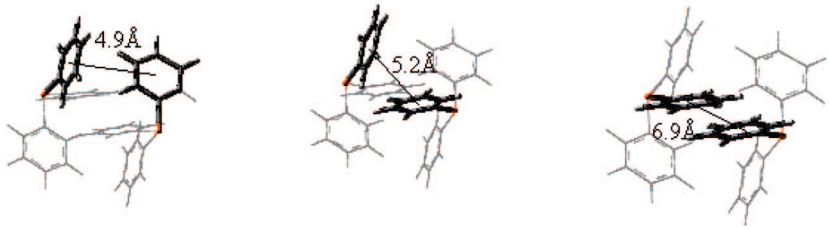

T-shaped Edge-edge Parallel-displaced

B. Intermolecular π-π stacking between triphenylphosphines along direction B

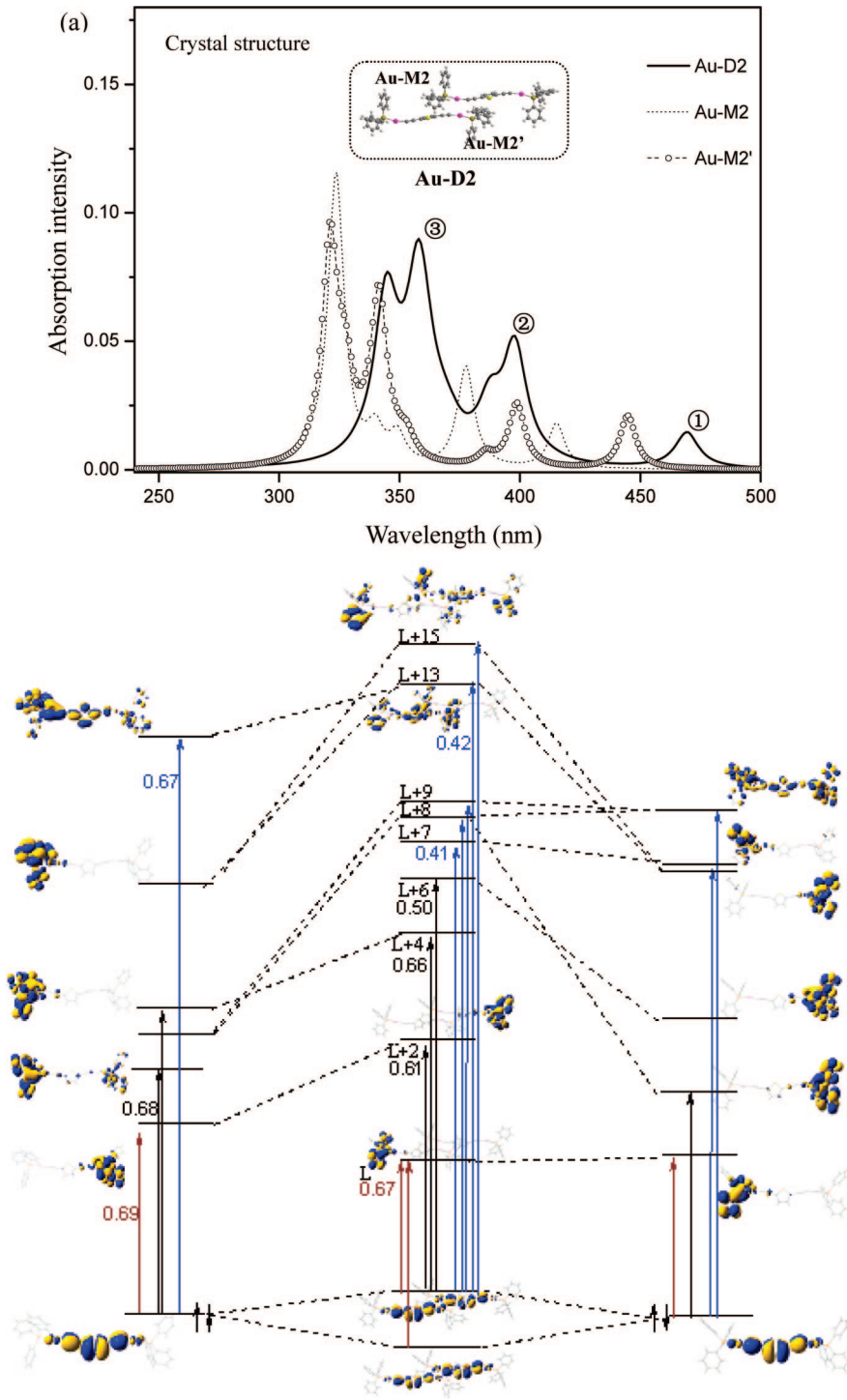

Figure 5. (a) UV−vis absorption spectra of gold phosphine acetylide monomers (**Au-M2**, **Au-M2′**) and dimer (**Au-D2**) in the crystal structure. (b) Energy correlation diagram for the formation of dimer **Au-D2** from the fragments **Au-M2** and **Au-M2′**, as well as the frontier molecular orbitals (taken at an isodensity value of 0.02 e·bohr^{-3}) involved in the low-lying transitions (which are marked in red, black, and blue arrowed lines, respectively). The coefficients of transitions are also given.

phase structure to a bending backbone in the crystal, two pronounced band shoulders appear at 308 and 297 nm, respectively, broadening the band III remarkably relative to the ligand-centered band II′ in the gas phase.

Substitution Effects. The influences of the substitution on the lowest excitation of gold acetylide and mercury acetylide in the gas phase are listed in Table 2. It can be seen that the lowest excitation energy of gold acetylide can be fine-tuned by ligand and metal substitutions. The absorption spectra of the gold complexes with different electron-withdrawing ligands, **Au-M2**−**Au-M5** (R = PPh_3, PMe_3, PH_3, and PF_3), display ligand-centered $\pi\pi^*$ transitions (band II′) in the range 351−403 nm. The red shift from **Au-M2** (R = PPh_3) to **Au-M5** (R = PF_3) is in accordance with the increasing electron-accepting ability of the substituent.

Upon changing the gold(I) center with isoelectronic mercury(II) (**Hg-M2**−**Hg-M5**, R = Ph, Me, H, and F), band II′ blue-shifts to 314−330 nm. In comparison with corresponding gold acetylides, the lowest excitation energies of mercury acetylide derivatives are less sensitive to the ligand substitution, with

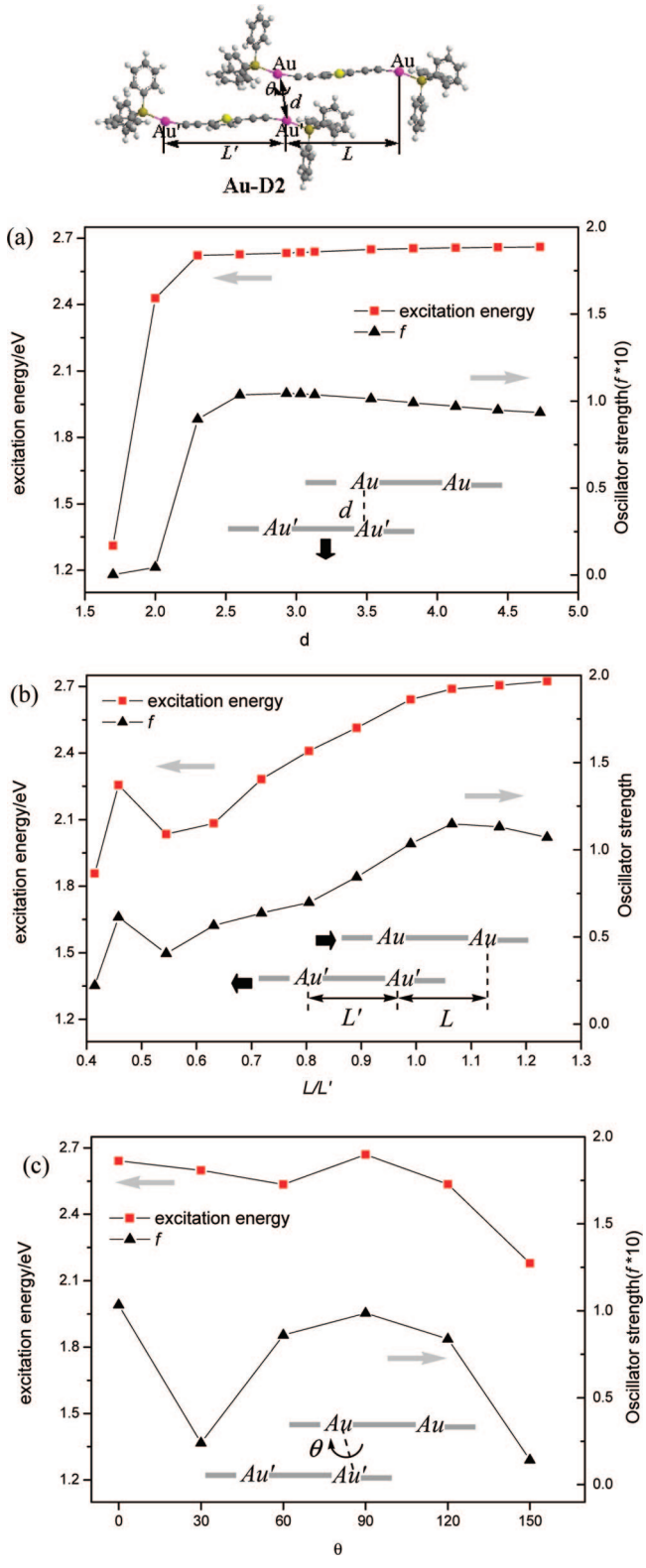

Figure 6. Lowest excitation energies and oscillation strengths (f) for **Au-D$_2$** as a function of (a) intermolecular Au···Au distance, d; (b) relative displacement, L/L', the ratio of horizontal displacements relative to one fixed monomer (e.g., $L/L' = 0$ corresponds an eclipse stacking); and (c) rotation angle, θ, around the Au−Au′ axis, respectively.

deviations in the maximum absorption between **Hg-M2** and **Hg-M5** less than 16 nm. This can be explained by the relative compositions of frontier molecular orbitals (shown in Table S4). The HOMOs and LUMOs of mercury acetylides have

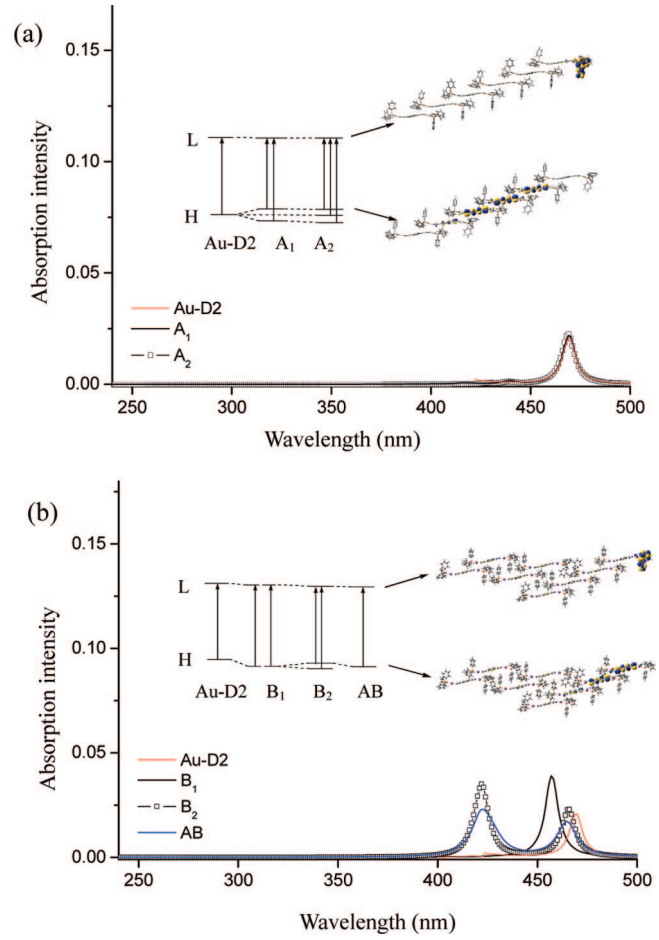

Figure 7. UV−vis absorption spectra of packing oligomers: (a) **A$_n$** (n = 1, 2), along Au···Au stacking (A) direction; (b) **B$_n$** (n = 1, 2), along $\pi-\pi$ stacking (B) direction as well as **AB** in a mixture of direction. The evolution of the energy levels of HOMOs (H) and LUMOs (L) with propagation in the crystal aggregates is also shown.

little contribution (less than 5%) from the ligand, R, in contrast to the large R components (up to 91.9%) in the LUMOs of gold acetylides.

3.2.2. Aurophilic Dimers: Influence of Packing Styles. The low-lying excitations of gold acetylides were suggested to belong to MLCT, LMCT, LLCT, MC (metal-centered charge transfer), LC (ligand-centered charge transfer), and MMLCT (metal−metal to ligand charge transfer), depending on the choice of ligand and style of crystal packing.[8] To study the stacking effects on spectra of dinuclear gold acetylide, **Au-D2** is adopted as the simplest model, which consists of two monomers (**Au-M2** and **Au-M2′**). For comparison, the mercury acetylide counterpart (**Hg-D2**) is also considered.

Dimer in Crystal Geometry. In Figure 5, the absorption spectrum of **Au-D2**, obtained by TDDFT calculations with the B3PW91 functional, is compared with those of constituent monomers **Au-M2** and **Au-M2′**. More details are given in Table S5. The low-lying dipole-allowed transition bands of **Au-D2** are marked as ①, ②, and ③, respectively. Band ① mainly comes from the HOMO → LUMO transition. Within the framework of semiemperical EHMO,[10a,d] DFT,[10e] or SCF-Xα-SW[10f] calculations, the Au···Au interaction was expected to lower the energy of the HOMO → LUMO transition, where the HOMO was assigned as the antibonding combination of the Au 5d orbitals or ligand π orbital, and the LUMO as the bonding combination of the Au 6s/6p orbitals or ligand π^*

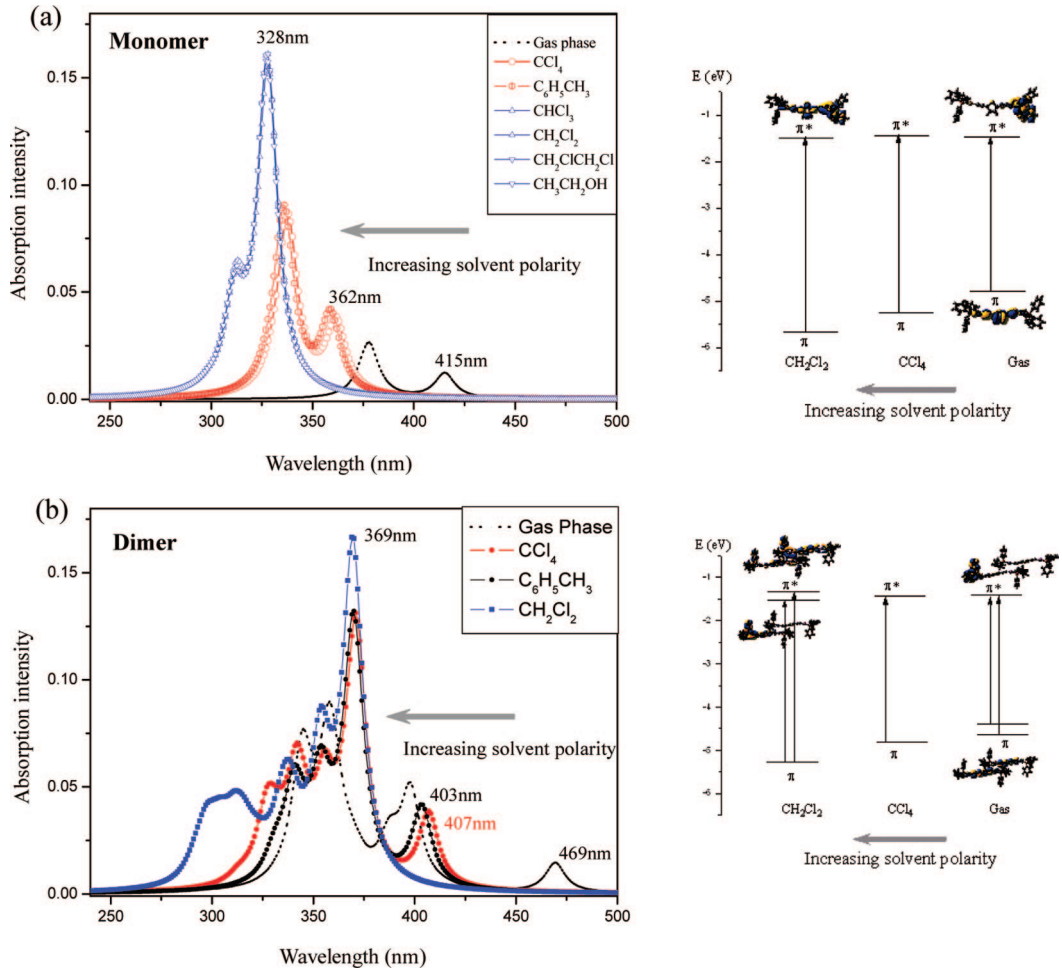

Figure 8. UV−vis absorption spectra for (a) monomer **Au-M2** and (b) dimer **Au-D2** obtained from TD-DFT/PCM calculations with the crystal structure in the gas phase and various dielectric media. The changes of energy levels of the frontier orbitals upon increasing solvent polarity are also illustrated.

orbital.[10] In **Au-D2**, due to the relative lower energy level of vacant $\pi^*(PPh_3)$, the lowest vertical excitation is mainly of LLCT character, mixing with some MMLCT. The second absorption band, ②, at 397 nm is broadened by a band tail at 388 nm, as is the transition band ③ (at 358 nm) of the dimer.

The influence of the intermolecular Au···Au interaction on the low-lying absorption bands can be qualitatively understood from the evolution of the frontier molecular orbitals from the constituent monomers (**Au-M2** and **Au-M2′**) to the dimer, as shown in Figure 5b. The lowest energy absorption band, ①, at 469 nm of dimer **Au-D2** is red-shifted relative to those of monomers (40 nm on average) due to the intermolecular aurophilic interaction.

In mercury acetylide, the change in the lowest excitation energy is to a much lesser extent from monomer **Hg-M3** to dimer **Hg-D2** than the gold counterparts, as shown in Figure S1b. Such a difference may come from the much stronger intermolecular metal−ligand interactions than the Hg···Hg interactions in mercury acetylide.

Different Packing Arrangements. We study the dimer **Au-D2** in various packing styles, such as a vertical move, horizontal displacement, and rotation around the Au−Au′ axis. Figure 6 presents the evolution of the lowest excitation energy and oscillation strength as a function of the intermolecular Au···Au distance, d, the extent of cofacial stacking, L/L', and the rotation angle, θ, respectively. The intermolecular Au···Au distance and horizontal slippage affect the lowest transition markedly. It can be found that as the effective Au···Au interactions increase (with short Au···Au distances and nearly cofacial packing), there is a decrease in the absorption maxima of the dimer. This can be rationalized from the variations in frontier orbitals with different stacking styles, as exemplified by the evolution of frontier molecular orbitals with Au···Au distances ranging from 1.73 to 4.73 Å in Figure S2.

3.2.3. Packing Oligomers. As noted above, evident red shift is observed in the lowest energy transition from the monomer **Au-M2** to dimer **Au-D2**. On going to higher oligomers in crystal packing of gold phosphine acetylide, there are two kinds of intermolecular interactions, aurophilic Au···Au and π···π stackings, along the A and B directions, respectively, as illustrated in Scheme 1. In this subsection, larger aggregates are selected from the crystal structure along A, B, and mixed AB packing directions, denoted as $\mathbf{A_n}$, $\mathbf{B_n}$, and **AB**, respectively, as shown in Figure 1b and Figure 7.

Packing along Au···Au Contacts. TDDFT/B3PW91 calculations indicate that the lowest dipole-allowed excitation energy is nearly unchanged in the propagation of Au···Au contacting from $\mathbf{A_1}$ to $\mathbf{A_2}$ along the A direction. In Figure 7a, the lowest absorption peaks of $\mathbf{A_1}$ and $\mathbf{A_2}$ are both predicted at 469 nm, nearly identical to that of dimer **Au-D2**. It is interesting to note that symmetric energy splitting of the HOMO levels is found in $\mathbf{A_n}$ as a result of intermolecular Au···Au interaction (Figure 7a). All the LUMOs of the studied oligomers are π^*-antibonding orbitals localized on the PPh_3 ligand with identical

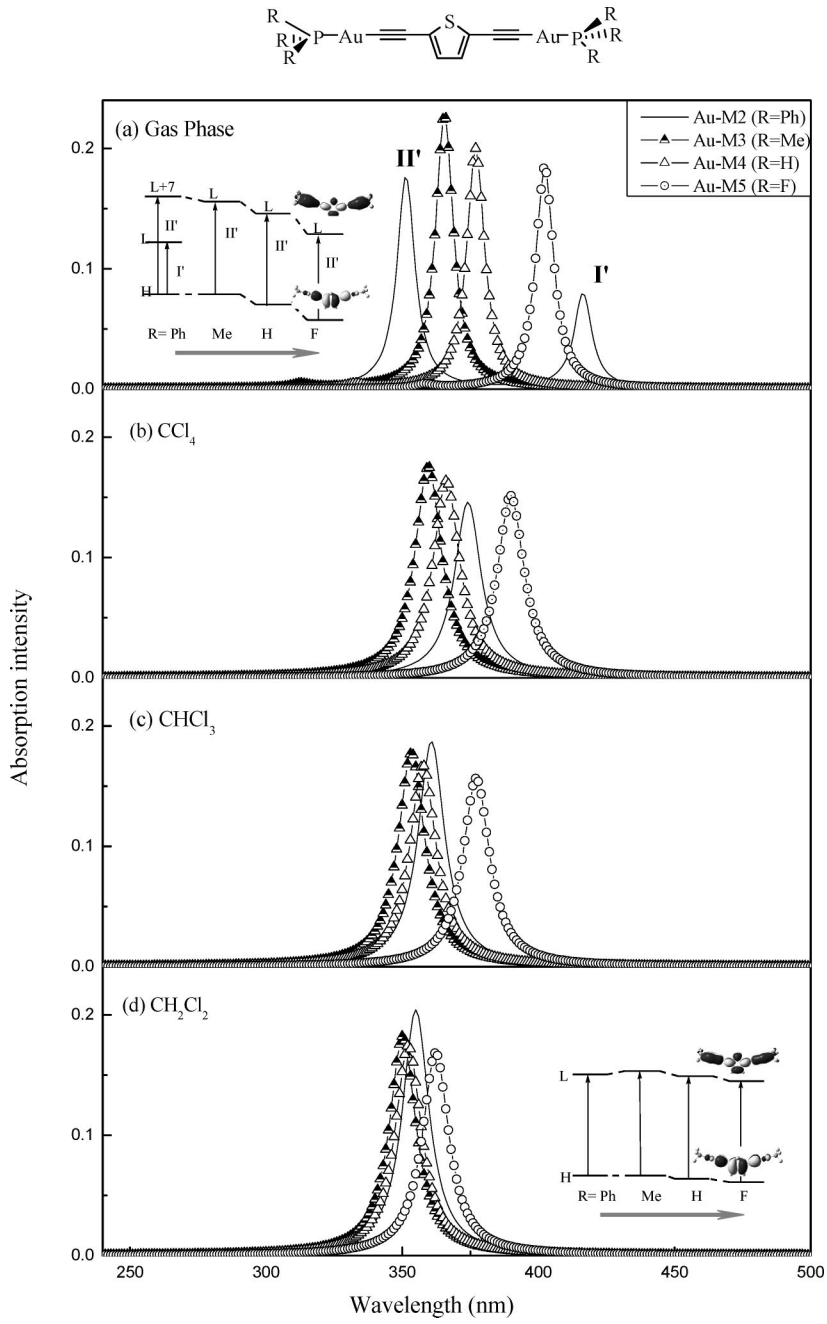

Figure 9. UV−vis absorption spectra of gold acetylides **Au-M2**, **Au-M3**, **Au-M4**, and **Au-M5** in (a) the gas phase; (b) CCl_4; (c) $CHCl_3$; and (d) CH_2Cl_2, obtained from TD-DFT/PCM calculations.

energy levels. This may partially explain the constant excitation energy on going from dimer **Au-D2** to tetramer $\mathbf{A_1}$ and hexamer $\mathbf{A_2}$ along the direction A.

Packing along $\pi-\pi$ Stacking. In the case of $\pi-\pi$ stacking along the B direction, a blue shift of 12 nm in the lowest transition energy is noticed when the model is enlarged from the dimer **Au-D2** to tetramer $\mathbf{B_1}$. Upon further elongation to the hexamer $\mathbf{B_2}$ and octamer **AB**, along the B and AB directions, respectively, the lowest excitation energies increase slightly. Similar to what is found in the dimer, the lowest excitations of $\mathbf{B_2}$ and **AB** are dominated by $\pi\rightarrow\pi^*$ transitions. Although the $\pi-\pi$ interaction between the PPh_3 moieties is predicted to be 10.5 kcal/mol at the MP2/6-31+G* level in the crystal structure, little influence from the $\pi-\pi$ stacking has been exerted on the lowest dipole-allowed excitation energies.

3.2.4. Solvent Effects. The low-lying vertical excitations of monomers and dimers in various solvents are evaluated by the TD-DFT/PCM calculations (shown in Figure 8 and Figure S3). The effects of ligand and metal substitutions on the absorption spectra of gold and mercury acetylides in different solvents are revealed in Table 2, with detailed illustrations of low-lying excitations of **Au-M2**−**Au-M5** and **Hg-M2**−**Hg-M5** depicted in Figures 9 and 10, respectively.

Monomers in Solutions. The UV−vis data for the constituent monomer **Au-M2** are not available, but there are experimental data for some related species.[8a] The predicted lowest excitation wavelengths of **Au-M2** in CH_2Cl_2 ($\varepsilon = 8.9$) with DFT and crystal geometries (355 and 328 nm, respectively) are comparable to the experimental maximum absorption of mononuclear $[(PPh_3)Au(C{\equiv}C(C_4H_2S)\ (C_4H_3S))]$ (354 nm) measured in dichloromethane solution.[8a]

The lowest dipole-allowed transition of **Au-M2** undergoes a blue shift upon increasing the solvent polarity. It can be seen from Figure 8a that the absorption maximum shifts from 415

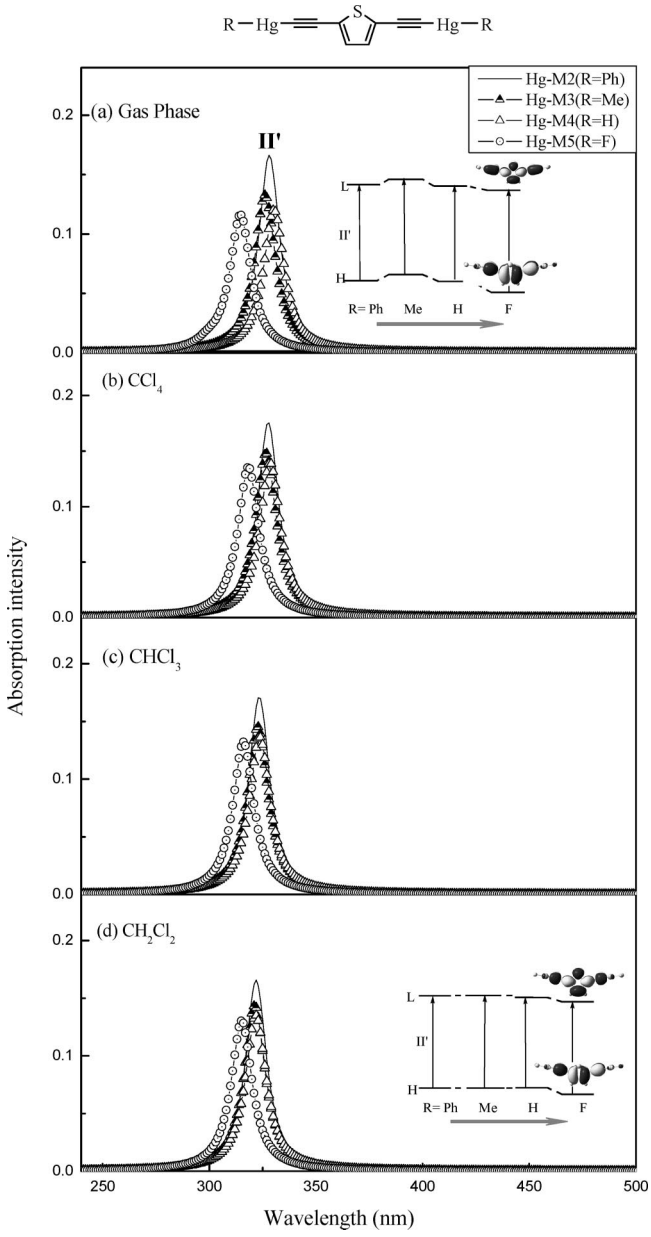

Figure 10. UV−vis absorption spectra of mercury acetylides **Hg-M2**, **Hg-M3**, **Hg-M4**, and **Hg-M5** in (a) the gas phase; (b) CCl_4; (c) $CHCl_3$; and (d) CH_2Cl_2, obtained from TD-DFT/PCM calculations.

to 362 and finally to 328 nm as the solvent polarity increases from gas phase to nonpolar CCl_4 ($\varepsilon = 2.23$) and $C_6H_5CH_3$ ($\varepsilon = 2.4$) and to weakly polar $CHCl_3$ ($\varepsilon = 4.9$), respectively. When the solvent polarity further increases from CH_2Cl_2 ($\varepsilon = 8.9$) to polar CH_2ClCH_2Cl ($\varepsilon = 10.36$) and to CH_3CH_2OH ($\varepsilon = 24.5$), the maximum absorption wavelength almost stays invariant at 328 nm.

The effect of substitution on the lowest excitation of gold acetylides is sensitive to the surrounding media. The deviation in absorption maximum decreases as the solvent polarity increases (Figure 9). However, from gas phase to polar solvent, the lowest excitation energies of mercury acetylides almost stay constant (Figure 10). The lowest transition energies of mercury derivatives are also insensitive to the ligand substitutions.

Dimers in CCl_4, $C_6H_5CH_3$, and CH_2Cl_2. The effects of solvent polarity on the lowest dipole-allowed transitions of dimers are similar to those of monomers. As shown in Figure S3, the lowest excitation energy of **Hg-D2** is invariant to the solvent polarity, while the lowest transition of **Au-D2** (Figure 8b) undergoes a significant blue shift of 62, 66, and 100 nm on going from the gas phase to nonpolar CCl_4 and $C_6H_5CH_3$ and to polar CH_2Cl_2, respectively.

On the basis of the analysis of molecular orbitals involved in the transition (Table S4), the calculated lowest excitation of dimer **Au-D2** in CH_2Cl_2 (369 nm) mainly corresponds to LLCT originated from the ligand-centered $\pi-\pi^*$ transition, mixing with some metal-centered d→p transition. For d^{10} metal complexes with aurophilic interactions, such metal-centered transitions are representative.[5g,8c,e,g,10c−e] Recently, a DFT/B3LYP (SDD for Au; 6-31G* for all other atoms) calculation was carried out on alkynyl gold aminodiphosphine with an intramolecular Au···Au distance of 2.840 Å.[10e] The lowest excitation energy was suggested to arise mainly from π(ArC≡C)→π^*(PNP) LLCT with some metal-centered dσ^*→pσ(Au) charge transfer character. The predicted maximum absorption wavelength of 369 nm for **Au-D2** agrees within 8 nm with the experimental maximum absorption of alkynyl gold triphenylphosphines in CH_2Cl_2 solution.[8a,10b] Similar ligand-centered $\pi\rightarrow\pi^*$ transitions in the near-UV region (344−370 nm) were also reported for d^{10} alkynyl mercury(II) phosphines[10b] and alkynyl gold(I) phosphines with a fluorene linking unit.[5i,10b]

4. Conclusion

The packing, substitution, and solvent effects on the low-lying excitation energies of gold and mercury acetylides have been investigated by using TD-DFT and TD-DFT/PCM methods. The low-lying excitation energies of gold acetylides in the solid state are calculated on the basis of a series of stacking aggregates, ranging from monomer to octamer. It has been demonstrated that the lowest dipole-allowed vertical excitation energy is red-shifted from the monomer to Au···Au linked dimer and then stays invariant as the stacking length extends along Au···Au (A) and $\pi-\pi$ contacts (B), as well as mixed AB directions. The solvent effects on the low-lying excitations of gold and mercury acetylides have been analyzed by calculations on the monomer, dimer, and a series of ligand- and metal-substituted metalacetylide derivatives in various solvents. The lowest excitation energies of mercury acetylides are insensitive to solvent polarity and ligand substitution due to the weak intermolecular Hg···Hg interactions, while TD-DFT/PCM calculations exhibit a remarkable blue shift in the lowest transition energy of gold acetylides as the solvent polarity increases. The lowest ligand-centered excitation of gold acetylides can be fine-tuned by varying the ligand and metal center. The media polarity has played a vital role in governing the lowest excitation energy, even for weakly polar solvents. The understanding of the relationship between intermolecular packing, solvent effect, and optical property may facilitate the improvement of the performance of gold and mercury acetylide-based materials.

Acknowledgment. This work was supported by the National Natural Science Foundation of China (Grants 20433020 and 20573050) and the Chinese Ministry of Education (Grant NCET-05-0442). One of the authors (Y.L.) also thanks NSF of China (20703008).

Supporting Information Available: DFT functionals used in this work (Table S1); geometrical parameters of gold and

mercury acetylide monomers (Table S2); TD-DFT singlet transition energies (E_{ex}) and oscillator strengths (f) for **Au-M2** and **Au-D2** in gas-phase and X-ray geometries (Tables S3 and S5); molecular orbital components of **Au-M2** derivatives and **Au-D2** (Table S4); lowest TD-DFT singlet transition energies (E) and oscillator strengths (f) for oligomers $\mathbf{A_n}$, $\mathbf{B_n}$, and **AB** (Table S6); frontier molecular orbitals involved in Figure 6a (Figure S2); singlet transition energies (E_{ex}) and oscillator strengths (f) for **Au-D2** in various solvents (Table S7); simulated UV−vis absorption spectra of **Hg-D2** and **Hg-M3** in the gas phase and various solvents (Figures S1 and S3). This material is available free of charge via the Internet at http://pubs.acs.org.

OM8001697